Biogeosciences Discuss., 6, 8167–8213, 2009
www.biogeosciences-discuss.net/6/8167/2009/

Biogeosciences Discussions

Biogeosciences Discussions is the access reviewed discussion forum of *Biogeosciences*

Mean vertical velocities and flow tilt angles at a fetch-limited forest site in the context of carbon dioxide vertical advection

E. Dellwik[1], **J. Mann**[1], **F. Bingöl**[1], **and K. S. Larsen**[2]

[1]Wind Energy Division, Risø National Laboratory for Sustainable Energy, Technical University of Denmark, Frederiksborgvej 399, 4000, Denmark
[2]Biosystems Division, Risø National Laboratory for Sustainable Energy, Technical University of Denmark, Frederiksborgvej 399, 4000, Denmark

Received: 3 July 2009 – Accepted: 24 July 2009 – Published: 12 August 2009

Correspondence to: E. Dellwik (ebde@risoe.dtu.dk)

Published by Copernicus Publications on behalf of the European Geosciences Union.

Abstract

An analysis of flow angles from a fetch-limited beech forest site with clearings is presented. Flow angles and vertical velocities from two types of sonic anemometers as well as a ground based remote sensing lidar were analysed. Instead of using rotations, where zero-flow angles were assumed for neutral flow, the data from the instruments were interpreted in relation to the terrain.

Uncertainties regarding flow distortion and limited sampling time (statistical uncertainty) were evaluated and found to be significant. Especially for one of the sonic anemometers, relatively small changes in the flow distortion correction could change the sign of mean vertical velocities taken during stable atmospheric stratification relative to the neutral flow. Despite the uncertainties, it was possible to some extent to relate both positive and negative mean flow angles to features in the terrain.

Conical and linear scans with a remote sensing lidar were evaluated for estimation of vertical velocities and flow angles. The results of the vertical conical scans were promising, and yielded negative flow angles for a sector where the forest is fetch-limited. However, more data and analysis is needed for a complete evaluation of the technique. The horizontal linear scans showed the variability of the mean wind speed field. A vertical velocity was calculated from different focusing distances, but this estimate yielded unrealistically high vertical velocities, due to neglect of the transversal wind component.

The vertical advection term was calculated using the measured mean flow angles at the mast and profile measurements of carbon dioxide, but it is not recommended to use in relation with the flux measurement as the vertical velocity measured at the mast is most likely not representative for the whole forest.

1 Introduction

Eddy covariance measurements, which provide a direct method of measuring turbulent fluxes of carbon to and from the land surface, are the main component in the FluxNet (Baldocchi et al., 2001) network of towers for assessing the terrestrial carbon balance. However, also the mean motion of the air may result in a net flux. This has been recognized in many studies on advection flows (Lee, 1998; Finnigan, 1999; Baldocchi et al., 2000; Paw et al., 2000; Feigenwinter et al., 2004; Aubinet et al., 2005; Vickers and Mahrt, 2006; Mammarella et al., 2007; Heinesch et al., 2007; Feigenwinter et al., 2008; Leuning et al., 2008; Yi et al., 2008; Kutsch et al., 2008).

The advective terms and their contribution to the net exchange of carbon are difficult to assess. For example, after enormous experimental effort, Feigenwinter et al. (2008) concluded that the advection terms should not be included for net ecosystem exchange of carbon on an hourly basis, due to excessive scatter. Heinesch et al. (2007) pointed out that the lack of precision of the of mean vertical velocity estimates was one of the main causes of the large uncertainty in the calculated vertical advection term. In a recent study, Leuning et al. (2008) stressed this point by stating a necessary accuracy for the mean vertical velocity of 1 mm s^{-1} in order to include the term at the short timescale. Such precision poses an extreme challenge, especially over forests, where the natural variations due to the turbulent nature of the flow are at 100–1000 times greater.

By comparing data from different instruments including both laser and sonic anemometry we try to assess the instrumental precision of determining mean vertical velocities. Using sonic anemometry, vertical velocities can be measured directly. Limitation to the precision of the sonic anemometer comes from flow distortion from the instrument itself as well as limited precision of the sonic transducer positioning and a possible temperature dependence of the transducer. The effect of flow distortion correction for sonic anemometry has previously been studied by Heinesch et al. (2007), but was analyzed in more detail here.

Whereas sonic anemometry has been extensively used for determining mean vertical velocities, laser anemometry is a novel technique. Lasers have been used to measure fluctuations of the vertical velocity (Lothon et al., 2006; Davis et al., 2009; Mann et al., 2009), but the mean vertical wind has never been reported. For the type of lidar (LIght Detection And Ranging) used in this study, the mean vertical velocity is calculated from conical scans of velocities along the beam direction, and the beam is focused at predefined heights. The mean wind speed field can then be estimated from the scans. However, if the terrain is not homogeneous and the flow field varies over the cone, the derived velocities will be biased. In comparison to a profile of sonic anemomter measurements of vertical velocity, the lidar has the advantage of measuring with the exact same tilt relative to the surface at all focus distances.

Common for measurements from both sonic anemometers and lidars is – as mentioned above – the inherent difficulty of assessing a precise mean value from a rapidly varying time series. This limitation to accuracy can be quantified by the statistical or stochastic uncertainty, which is estimated using the ratio of the natural variation and the length of the time series (Lenschow et al., 1994). In this study, the statistical uncertainty was estimated for varying stability conditions.

With vertical velocity, we mean the velocity component parallel to the force of gravity. For a flat and homogeneous site covered with low vegetation, the velocity component normal to the mean flow will coincide with the vertical velocity. In this case, the mean flow follows the terrain and the flow angle during neutral atmospheric stratification is zero. This fact can be used to compensate for the limited instrumental precision of measurement instruments, by letting the measured neutral flow define the surface over which the mean vertical flow is zero.

For forests, the surface defined by the level of maximum drag in the canopy crown space, which is closely related to the displacement height (Thom, 1971), may or may not be parallel to the ground surface due to variable tree height, thereby adding a level of complexity to the flow. For more complex sites, where either clearings are present, the fetch is limited or the terrain itself is complex, the neutral flow may not follow neither the ground surface nor the surface defined by the tree crowns, since the flow is still adapting to the inhomogeneities.

With an implicit focus on the instrumental limitations, it has however been common in advection studies to define an empirical reference surface, which in turn defines the direction of the vertical flow component. The definition of this empirical surface is based on the wind measurements, regardless if the flow can be expected to follow the terrain or not. Finnigan (1999) recommended that only measurements taken during near-neutral atmospheric stratification should be used for defining this plane, whereas it also has been common to use all measurements. Once this reference plane has been defined, mean vertical velocities relative to the plane can subsequently be calculated for each measurement run.

Generally, two types of rotation methods have been used for defining a reference plane from the measured wind field: (1) Sinusoidal and offset corrections are applied to measured data, which compensates for a tilt between the underlying surface and the plane defined by the sonic coordinate system as well as an arbitrary off-set (Baldocchi et al., 2000; Paw et al., 2000; Feigenwinter et al., 2004). (2) The reference plane is made up of cake slice shaped planes, where each sector is intended to be parallel to the underlying surface in the corresponding wind direction. Such an approach has been used by Lee (1998); Mammarella et al. (2008); Feigenwinter et al. (2008); Kutsch et al. (2008) and Yi et al. (2008).

Method 1 corrects for a potential misalignment of the sonic anemometer relative to the underlying surface as well as compensates for an off-set. Method 2 would, as well as remove sonic tilt effects and instrumental off-sets, also remove any systematic vertical velocity caused by i.e. flow distortion from mast and booms as well as local effects from clearings, roughness changes and non-flat terrain. If a systematic off-set in measured flow angles is caused by the terrain rather than the instrument, the effect of the local terrain of the flow is also removed by method 1.

The above methods are similarly described in Paw et al. (2000), who also list a third method which is the one we attempt in this study; namely to relate the measured vertical velocities and flow angles to the terrain in the area of the footprint for the measured flux. The main reason for using this method is that at the study site, the flow angles can not be expected to follow the terrain due to both heterogeneities within the forest as well as a limited fetch.

The measurement site in focus for this study is located in a flat and fetch-limited beech forest surrounded by agricultural fields near the municipality of Sorø, Denmark. Influence from the fetch limitation has previously been studied at this site (Dellwik and Jensen, 2000, 2005; Mammarella et al., 2008), where the presence of both an internal boundary layer as well as a roughness sublayer were demonstrated and investigated. Vertical velocities in connection with a roughness change have previously been studied by Vickers and Mahrt (2006). They investigated the horizontal and vertical advection components in a 300 m×300 m large plantation of young pine trees surrounded by taller trees. Compared to their study, the roughness change at our site is larger and of reverse sign (from smooth to rough terrain). Vickers and Mahrt (2006) introduced a fourth method to deduce the mean vertical velocities in an advection study, which is based on careful measurements of the horizontal wind components. Using the continuity equation, the vertical velocity can be deduced from divergence in the horizontal wind field. Compared to methods 1 and 2, no assumption about whether the mean neutral flow angle is equal to zero is necessary. The same method has hence been used by Leuning et al. (2008) and Heinesch et al. (2007). Since the lidar campaign at the Sorø site included a period where the horisontal variability of the mean flow was measured by mounting the lidar head directly on the mast, this approach was also tested.

Lee (1998) proposed several possible sources for vertical mean velocities, which are caused by large scale temperature driven atmospheric motions. Near the surface, it was estimated that these temperature-driven vertical velocities are of the order mm s^{-1} to cm s^{-1}. Lee assumed that flux sites are located in homogeneously vegetated and flat terrain, in which case local effects on the vertical flow would be negligible. By calculating the vertical velocities relative to the defined reference plane, one would therefore directly be able to assess the large-scale driven vertical motions and estimate their impact on the carbon budget.

For the more non-ideal sites, where carbon dioxide advection studies have taken place, the interpretation of positive or negative flow angles relative to the reference plane is less straight-forward. The estimated vertical velocities can then only represent large scale temperature driven vertical motions described by Lee (1998) if one assumes that the topography effects and the stability effects can be separated. This assumption is problematic especially over forested terrain, where – in addition to the relatively large natural variability of a forest – specific canopy-flow features such as flow separation already at moderately sloped forested hills (Sogachev et al., 2004; Belcher and Hunt, 1998) and separation of the above/below canopy flow (Smith et al., 1972; Belcher et al., 2008) are typically expected to vary with atmospheric stability.

The aim of this paper is to understand the most crucial uncertainties related to measured vertical velocities, the possible effect of inhomogeneity on the vertical velocities and what the implication is for determining the vertical advection term in the carbon dioxide mass conservation equation at sites influenced by surface inhomogeneities. Finally, the possibility of using remotely sensed vertical velocities by lidars is evaluated based on field experiment data.

2 Theory and initial lidar evaluation

2.1 Expected effect of forest edge on vertical velocities

We hypothesize that the atmospheric flow encountering a perfect two-dimensional forest edge, may be described by the following phases (Fig. 1):

1. Edge phase: At the forest edge, the mean flow is dominated by the physical effect of the edge, which accelerates the flow above the canopy and decelerates the flow within the canopy. Both above and below the crowns, the mean vertical velocity W is positive. Above the canopy W decreases with height and within the canopy W increases with height.

2. Deceleration phase above the canopy: At canopy height h_C, the mean wind speed U starts decelerating ($\frac{dU}{dx}|_{h_C}$=0), due to the high roughness and a roughness sublayer as well as an internal boundary layer develop. The mean wind speed in the canopy (U_C), reaches its minimum value $U_{C,\min}$. W is, due to continuity, slightly positive within the canopy. Above the canopy W is positive nearly zero, but increases slightly with height. The end of phase 2 is defined by $W(h_C)$=0.

3. Interaction phase: The roughness sublayer is now deep enough to produce large-scale eddies which can penetrate into the canopy. Any interaction between the two flows will result in an acceleration of the flow in the canopy, which, again using the continuity argument, will result in negative values of W.

4. Equilibrium phase ($W(h_C)$=0): There is no net vertical motion between the below-canopy and above canopy regions as the below canopy flow and the above canopy flow are in equilibrium. The internal boundary/equilibrium layer is deep and effects from the edge are of no importance.

Experimental support for the existence of phases 1, 2 and 3 was presented by Irvine et al. (1997), who reported positive flow angles near the edge of a dense Sitka spruce plantation, a slight speed-up of the flow at the edge for the height $2h_C$ at x=3.5h_C, flow deceleration at h_C for x<14.5h_C and negative flow angle of -2.5° at x=14.5h_C at the height of $2h_c$, where x is the distance from the measurement position to the upwind edge and h_C is the canopy height. However, at x=14.5h_C, flow angles within the canopy was still positive and near-zero within the canopy and at the canopy top respectively, which would point towards an acceleration of the flow above canopy, rather than interaction between the above and below canopy regions. For a $k-\varepsilon$ closure Reynold's averaged CFD model, a study by Sogachev et al. (2008) showed negative vertical velocities in the region of $25h_C<x<40h_C$ near the canopy top.

Negative flow angles could also occur as an effect of limited extension of the forest. The forest edge wind-tunnel study by Morse et al. (2002) indicated negative vertical velocities from $x>7h_C$ near the canopy top, which could be an effect of the limited extension of $12h_C$ of the forest. In the large eddy simulation modelling study by Yang et al. (2006), negative flow angles were present from $x>11h_C$ above the canopy where the trailing forest edge was located at $x=19h_C$. In contrast, the LES study by Cassiani et al. (2008) did not report any negative flow angles near canopy height for a forest block of the horizontal extension $25h_C$.

2.2 Statistical uncertainty of the mean vertical velocity

The relationship between averaging time T and statistical uncertainty expressed as the variance of mean vertical velocity $\sigma^2_{W_T}$ can be stated from i.e. Lenschow et al. (1994) as follows

$$T = 2\frac{\sigma_w^2}{\sigma_{W_T}^2} \cdot \tau_W = 2\frac{\sigma_w^2}{\sigma_{W_T}^2}\frac{L_W}{U}. \tag{1}$$

Here, σ_w^2 is the variance of the instantaneous vertical wind speed w and τ_W is the integral time scale of the vertical velocity fluctuation. The time scale is expressed as the ratio of the vertical length scale L_W and the mean horizontal velocity U. Equation (1) is re-arranged to

$$\sigma_{W_T} = \sigma_w\sqrt{\frac{2L_W}{TU}} \tag{2}$$

From Eq. (2), the uncertainty of the mean flow angle α can be derived as:

$$\sigma_{\alpha_T} \approx \frac{\sigma_{W_T}}{U}. \tag{3}$$

For the calculations in this study, $L_W \approx z_m - d$ where z_m is the measurement height, d the displacement height and σ_w and U are associated with mean values of measured data for different atmospheric stratification.

2.3 Vertical velocity measured by lidar in the conically scanning mode

We currently work with two types of lidars, that potentially can measure the vertical average velocity. Both instruments are developed for measuring profiles of horizontal velocity and direction with high precision and over long periods in the context of wind resource estimation. One, the ZephIR developed by QinetiQ, UK and produced and sold by Natural Power (UK), is a homodyne, continuous wave laser Doppler instrument that determines the range by focusing (Smith et al., 2006). The other, called WindCube, is a heterodyne pulsed lidar produced by Leosphere, France (Courtney et al., 2008).

In the conically scanning mode, the wind vector is determined from the lidar by fitting a trigonometric function to the velocity component in the beam direction over circle, defined by the cone edge, at predefined focus distances. Usually it is assumed that the wind field is homogeneous in space, but here we allow for a linear variation in space. Without loss of validity the analysis is ignoring the fact that the QinetiQ lidar only measures the magnitude of the radial wind speed, not the sign.

Assume the mean wind field $\boldsymbol{U}=(U,V,W)$ to vary linearly

$$U_i(\boldsymbol{x}) = U_i(\mathbf{0}) + x_j \frac{\partial U_i}{\partial x_j} \tag{4}$$

over a volume enclosing the lidar scanning circle. The origo of the coordinate system $\boldsymbol{x}=\mathbf{0}$ is the center of the scanning circle elevated by h over the instrument. Let

$$\boldsymbol{n} = (\cos\theta \sin\varphi, \sin\theta \sin\varphi, \cos\varphi) \tag{5}$$

denote a unit vector in the direction of the laser beam, where φ is the half opening angle of the cone and θ the azimuthal angle. In a homogeneous flow field, the along beam wind speed component, v_r, measured at an azimuthal angle θ is the projection of $\boldsymbol{U}$ onto $\boldsymbol{n}$ as given by Eqs. (4) and (5):

$$v_r(\theta) = \boldsymbol{n}(\theta) \cdot \boldsymbol{U}\left(\boldsymbol{n}(\theta) l - (0, 0, h)\right), \tag{6}$$

BGD

6, 8167–8213, 2009

Mean vertical velocities and flow tilt angles at a fetch limited forest site

E. Dellwik et al.

where the velocity field is evaluated in the position of the focus of the laser beam. Here $l = h/\cos\varphi$ is the focus distance. The additional variations of v_r due to lack of homogeneity may be expressed as $v_r'(\theta) = v_r(\theta) - \boldsymbol{n}(\theta)\cdot\boldsymbol{U}(\boldsymbol{0})$, and it can be written in terms of the velocity gradient:

$$v_r'(\theta) = n_i(\theta)\left(n_j(\theta)l - \delta_{j3}h\right)\frac{\partial U_i}{\partial x_j}. \tag{7}$$

Substituting (5) into this equation and ordering the terms as a Fourier series in θ we finally get

$$\begin{aligned} v_r(\theta) = {} & W\cos\varphi + \frac{l}{2}\sin^2\varphi\overbrace{\left(\frac{\partial U}{\partial x} + \frac{\partial V}{\partial y}\right)}^{=-\partial W/\partial z} \\ & + \sin\varphi\left(U + l\cos\varphi\frac{\partial W}{\partial x}\right)\cos\theta \\ & + \sin\varphi\left(V + l\cos\varphi\frac{\partial W}{\partial y}\right)\sin\theta \\ & + \frac{l}{2}\sin^2\varphi\left(\frac{\partial U}{\partial x} - \frac{\partial V}{\partial y}\right)\cos 2\theta \\ & + \frac{l}{2}\sin^2\varphi\left(\frac{\partial U}{\partial y} + \frac{\partial V}{\partial x}\right)\sin 2\theta \quad . \end{aligned} \tag{8}$$

The horizontal and vertical wind speeds are derived from the lidar measurements by fitting a trigonometric series $a + b\cos\theta + c\sin\theta$ to the data. The vertical wind speed is then estimated as $a/\cos\varphi$ while the horizontal components are $b/\sin\varphi$ and $c/\sin\varphi$, respectively. In the presence of a linear deviation from homogeneity we thus get for the wind vector estimated from the lidar:

$$U_{\text{lidar}} = U + h\frac{\partial W}{\partial x} \tag{9}$$

$$V_{\text{lidar}} = V + h\frac{\partial W}{\partial y} \tag{10}$$

$$W_{\text{lidar}} = W - \frac{h}{2}\tan^2\varphi\frac{\partial W}{\partial z} \quad . \tag{11}$$

The last Eq. (11) was obtained by isolating all terms in Eq. (8) that were independent of on θ and then dividing the result with $\cos\varphi$

As a result of these equations, the error due to inhomogeneity of the mean flow will disappear for the vertical component as the half opening angle φ goes to zero, but the errors on the horizontal components are independent of φ. For the ZephIR lidar, φ=30.4° and if we assume $W/z \approx \partial W/\partial z$ and $h \approx z$, W_{lidar} will deviate 17% from the real W. The systematic error in the horizontal velocity due to inhomogeneity has been analyzed in more detail in Bingöl et al. (2009).

2.3.1 Tests at Høvsøre

Suppose that the mean vertical velocity is zero, the statistical uncertainty of $W_T \equiv \frac{1}{T}\int_0^T w(t)dt$ measured, for example, by the sonic is given by Eq. (2). The stochastic variation in the vertical velocity measured by the lidar is probably not very different. For a measurements period of 10 min, this implies for the flow angle α that $\sigma(\alpha_T)$=0.4° for low turbulence conditions (σ_w/U=0.05) and $\sigma(\alpha_T)$=0.7° for high turbulence conditions (σ_w/U=0.1). For a measurement period of 30 min the corresponding numbers are 0.2° and 0.4°.

These estimates are probably too optimistic for the lidar, since it does not measure continuously for thirty minutes. Instead, the beam is turned one round per second measuring three rounds at each focus height. If five heights are measured, each height is scanned for three seconds every fifteen seconds. This paused or disjunct sampling was studied for fluxes by Lenschow et al. (1994), who found that as long as the sampling cycle is shorter than the integral time scale, the statistical uncertainty does not increase significantly. However, here the sampling cycle is probably larger than the integral time scale implying a larger statistical uncertainty.

We want to investigate whether the estimates presented in the beginning of this subsection were of the right order of magnitude by looking at measurements from a very flat site. The Høvsøre test site operated by Risø DTU is ideal for that purpose (Smith et al., 2006). Høvsøre is situated 1.5 km from the North Sea on the west coast of Denmark in a very flat, rural area. The site has seven masts equipped with anemometers and other meteorological sensors measuring temperature, pressure, precipitation etc. The southernmost mast is the most well equipped with cup anemometers at 10, 40, 60, 80, 100, and 116.5 m and Metek sonic anemometers at 10, 20, 40, 60, 80, and 100 m. The cup and sonic data were stored almost continuously at 5 Hz and 20 Hz, respectively, since 2004. The lidars investigated here were located close to the mast. More information about the site may be found in Smith et al. (2006).

The data shown in Fig. 8 are 30 min averages of the vertical velocity measured by a ZephIR close the meteorological mast at Høvsøre as a function of wind direction. Wind coming from the north may be disturbed by the five large turbines on the test stand. Between the gray vertical lines the lidar is undisturbed by the turbines. A misalignment of the instrument with respect to the vertical direction will give a spurious sinusoidal variation of the vertical wind speed with direction. Such a variation with an amplitude of 0.5° was observed for the highest focus distance and was subtracted from all focus distances. Subsequently, the mean vertical wind speed was close to zero for all directions and heights, except 38 m, and the scatter around zero on the half hour values is approximately 0.25°. The deviation of the mean at 38 m cannot be explained at present. In conclusion, for a perfectly aligned instrument the scatter in the vertical flow angle is close to the theoretical estimates given in the beginning of this subsection.

Preliminary investigations of the Windcube showed that there were small offsets in the vertical velocity. They may be attributed to the acousto-optical modulator in that instrument, which offsets the zero Doppler shift such that the sign of the wind velocity along the beam can be derived. Since we do not have WindCube measurements over a forest, we do not pursue this issue in more detail.

3 Material and method

3.1 Site

The vegetation at the Sorø site (55°29′09″ N, 11°38′41″ E) on the island of Zealand, Denmark, consists predominantly of an 85 year old beech forest with a rather uniform height of about 26–27 m. The standard setup at the 57 m tall mast and 25 m tall scaffolding tower 8 m north of the mast, as well as general site information, can be found in Pilegaard et al. (2003). Information about fetch limitation and how it influences the wind and temperature profile at the mast position was discussed in Dellwik and Jensen (2005).

For the current focus on flow angles and vertical velocities in relation to the terrain, a terrain map is presented in Fig. 3 (left) where the full line shows the outline of the forest. The forest is located on almost flat terrain with a an inclination of ≈0.5° from the SW to the NE. Each height contour in the graph signifies 2 m height differences. Height profiles from aerial photography taken in 1995 (Dellwik and Jensen, 2005) indicated that the local variation of canopy height is much greater than the ≈0.5° over distances of ≈10 m. Over longer distances however, the canopy height may compensate for the slope, such that a general direction of the canopy top inclination is hardly distinguishable.

To the right of Fig. 3, an aerial photography from 2006 is shown (courtesy to Google Earth). The complex nature of the vegetation cover is clearly visible. The numbers in the Figure refer to the following features: 1. $8h_C$ to a large clearing in the direction of ≈60° from the mast, 2. Narrow strip of $17h_C$ homogeneous beech forest to forest edge in ≈90°, 3. $4h_C$ to a 15m tall planation of Norway Spruce in 155°, 4. $13h_C$ to a clearing in 200°, 5. $10h_C$ to another 15 m tall plantation of Norway Spruce in 245°, 6. $17h_C$ to the forest edge in 260°, 7. $9h_C$ to a clearing with younger beech of 5-6m height in 315° and finally 8. $26h_C$ to the forest edge in 360°.

The above stated distances to clearings, inhomogeneous surface cover and forest edges were assessed using Google Earth, as the distance from the mast to the first step change in vegetation height. The directions from the mast to the clearings/change of vegetation are approximate, given the relatively large transversal extension of the terrain features.

The leaf area index (LAI) at the Sorø beech forest site shows a strong intra-annual pattern, characterized by a low value during winter, a sharp transition to a high leaf area index around 1 May and a slow descent back to winter values in October–November. Between the beginning of June to the end of August, LAI is near constant and approximately 5 $m^2\,m^{-2}$. During no-leaf conditions LAI is approximately 1 $m^2\,m^{-2}$. These values are based on measurements by a LAI-2000 PCA (Li-Cor, Nebraska, USA).

The displacement height was estimated to be 21 m based on earlier analysis of the wind profile (Dellwik and Jensen, 2005) as well as an estimate of forest height to approximately 26–27 m.

The mast has a diameter of 30 cm and the instruments are mounted on 2 m long booms pointing towards 310°. For the eddy-covariance system at Sorø, a Solent 1012 R2 (Gill Instruments Ltd.) at 43 m height and a LiCor 7000 (Li-Cor, Nebraska, USA) were employed. The measurement record of carbon dioxide and water vapor fluxes started in 1996 and has run continuously since then. A profile system for measurement of carbon dioxide was operational from the spring of 2007 after a longer break. The carbon dioxide concentrations were measured at 0.1, 0.5, 1, 5, 15, 30 and 41 m above the soil surface via a series of Teflon tubes (inner diameter 4.8 mm) installed on the mast. One height at a time was sampled for 90s and the different heights were sampled in a step-wise order to ensure that all heights were measured at least twice per 30 min interval. The carbon dioxide concentrations were analyzed on an ADC-7000 infra-red gas analyzer, see (Pilegaard et al., 2003) for more details.

3.2 Experiments

For this study, data from several experiments were analysed. The duration and instrumentation are listed in Table (1).

3.2.1 Sonic anemometers

In order to assess the instrumental precision of sonic anemometry for mean vertical velocities, periods where both the eddy-covariance Solent R2 sonic anemomter and a USA-1 Basic (Metek Gmbh) at 31.5 m height were operational. Both the Solent R2 and USA-1 sonic heads are designed with the acoustical transducers on a vertical rod. The rod of the Gill sonic is 52cm and the sonic head has the dimensions 24×23 cm including supporting rods. The sound path is 14.9 cm. The USA-1 sonic head is slightly larger with the dimensions 32×24 cm with no supporting rods and the vertical bar is 47 cm. The length of the sound path is 17.5 cm.

Sonic anemometers by Gill are calibrated individually in a wind tunnel and corrected for flow distortion from the sonic structure itself, but only for wind attack angles up to 30° relative to the horizontal. It has been shown (Gash and Dolman, 2003), that over high roughness areas, such as forests, eddies hit the surface at a much steeper angle than over low-roughness terrain, and that the limited calibration was a likely cause for underestimation of surface energy fluxes. Following the work of Gash and Dolman (2003), van der Molen et al. (2004) developed a new sonic calibration scheme based on wind tunnel data for attack angles up to 90° for Gill R2 and R3 sonic anemometers. This correction scheme has hence been numerically improved by Nakai et al. (2006) to account more rigorously for the fact that the angle of attack, which is calculated from the measured wind vectors, also contains an angle of attack error. Apart from this numerical improvement of the correction scheme, the Nakai et al. study also included an updated correction for near-zero flow angles. The effect of the sonic calibration presented in van der Molen et al. (2004) has to some extent previously been examined by Heinesch et al. (2007), but these effect have otherwise been ignored. Both van der Molen et al. (2004) and Nakai et al. (2006) provide add-on corrections for the R2 design for all angle of attacks that can be downloaded from home pages listed in Nakai et al. (2006). These schemes were applied to the measured data.

The USA-1 basic sonic has a built-in calibration for flow distortion at zero-angle of attack. Metek Gmbh further provides a correction scheme for the instrument in the interval of -50° to $+45^\circ$ angle of attack on demand. This correction has to be applied to the raw data, such that the corrected data in this study are first de-corrected for the built in correction and then re-corrected with the -50° to $+45^\circ$ correction. For attack angles outside the calibration interval, the end point values were applied.

3.2.2 Lidar experiment

Between late August 2006 and January 2007, the ZephIR lidar was mounted on the scaffolding tower near to the mast, where it was used in the conically scanning mode described in the previous section. The height of the lidar head was estimated to 26 m and the focusing heights 24 m, 33 m, 41 m, 52 m, 68 m, 89 m, 116 m and 151 m were chosen.

During January and February 2007, the lidar head was mounted on the mast. With this setup, the lidar measures the wind component in the direction of the lidar beam for a fixed wind direction. This mode of running the lidar is referred to "linear" in the text. This experiment was designed to determine the spatial variation of the mean wind speed above the canopy. During mid-end of January the lidar was mounted at 38 m height with the beam pointing towards 270°.

3.3 Data processing and screening

Data were analyzed for both the summer and winter period. For the leaf-on period data between 1 June and 31 August were selected, and for the leaf-off period, data between 18 January and 1 April were selected. These periods are referred to "summer" and "winter" respectively. The limits of the periods were decided either by strict constancy of leaf area or availability of data from both sonic anemometers.

The data were block averaged over 30 min intervals and the sonic data were calculated using only one sonic rotation (alignment with the mean wind direction). For the heat and momentum fluxes, the difference between this single rotation scheme and

BGD
6, 8167–8213, 2009

the more traditional double rotation McMillen (1988) was assessed and considered negligible.

As mentioned above, the Sorø site has been operational since 1996. In an initial analysis, the flow pattern's dependence on wind direction was checked for all years. It was found that during the first four to five years of experiment, the flow tilt angle showed a sinusoidal dependence on wind direction, which could be explained by a misalignment of the sonic relative to the surface. However, from 2002 onwards the flow angles show a different pattern, which can not directly be linked to sonic misalignment. The change in sonic flow angle pattern is most likely an effect of a change of instruments.

Initially, we assume that the measured vertical data represent the flow parallel to the acceleration of gravity and perpendicular to the underlying surface. The real deviations and their possible effect on the interpretation of the measured data is discussed in Sect. 5.

For all neutral data it was required that $|\frac{z_m-d}{L}|<0.1$ and that $U_{z_m}>3\,\mathrm{ms}^{-1}$, where z_m=43 m. Especially during the winter time, the Metek sonic showed irregular instrumental failures possibly due to precipitation and further screening was necessary. These were $U_{43\,\mathrm{m}}>U_{31\,\mathrm{m}}$, $\sigma_W^2>0.03\,\mathrm{m}^2\,\mathrm{s}^{-2}$ and finally less than 10 samples were removed by requiring flow tilt angles to be less than 6°. Data not fulfilling this last criterion were typically taken immediately before or after instrumental failures. This procedure left 2150 samples for the summer period and 3347 samples for the winter period. For summer data, stability effects were examined, both in relation to the statistical uncertainty analysis (Eq. 2) and for interpreting the dependence on the terrain. In these analyses, it was required that $(z_m-d)/L<-0.1$ (unstable) or $(z_m-d)/L>0.1$ (stable) and $U_{z_m}>1\,\mathrm{ms}^{-1}$ (both unstable and stable).

A subset of the summer data was selected for 10Hz time series analysis. Here the criteria were sharpened as follows: wind directions should be in the interval [250°, 280°] to provide a uniform fetch, $|\frac{z_m-d}{L}|<0.01$ (near-neutral subset), $-0.5<\frac{z_m-d}{L}<-0.1$ (unstable subset), $0.1<\frac{z_m-d}{L}<0.5$ (stable subset)

These sharpened stability criteria left 50 near-neutral, 45 stable and 19 unstable of

BGD
6, 8167–8213, 2009

30 min averaged measurement runs.

4 Results

4.1 Statistical uncertainty

Following Eq. (2), mean values of measured σ_w and U were calculated and the statistical uncertainties σ_{W_T} and σ_α were evaluated for T=1800s (Table 2). The statistical uncertainty σ_{W_T} was of the same order of magnitude as the measured mean value of the absolute vertical velocity $|W_{\mathrm{Solent}}|$. There was a clear dependence on atmospheric stability with the greatest uncertainties associated with the unstable subset.

4.2 Effect of sonic flow angles and flow distortion corrections

Before applying the flow distortion correction, the attack angle probability density function ("pdf") on the Solent sonic were calculated as $\arctan \frac{w}{\sqrt{u^2+v^2}}$, where v denotes the instantaneous transversal wind component (Fig. 4, left). Similarly, the pdf for vertical wind speeds were evaluated using 10 Hz data (right).

The attack angle distribution during unstable atmospheric stratification was wider than for the neutral subset, which in turn was wider than the stable subset. The maximum values of W are generally higher during neutral conditions than during stable/unstable atmospheric stratification. The maximum measured value of W for this 10 Hz subset of summer data was around 7 ms^{-1}.

The effects of the sonic flow distortion corrections are shown in Fig. 5, where mean daily courses of W are presented. For this analysis, all data with $U_{43\,\mathrm{m}}$>1 ms^{-1} were used. The flow distortion correction led to a different daily course for the Gill R2 sonic measurements, whereas the weaker daily course for the Metek USA-1 sonic was preserved. For the Solent R2 anemometer, the "corr 1" and "corr 2" corrections correspond to the corrections presented by van der Molen et al. (2004) and Nakai et al.

(2006). Both flow distortion corrections for the Gill sonic led to a negative shift of vertical velocities, whereas the flow distortion correction for the Metek resulted in a positive shift of the vertical velocities. The Solent vertical velocities were changed on average 0.09 $\mathrm{m\,s^{-1}}$ and the USA-1 signals were changed 0.013 $\mathrm{m\,s^{-1}}$. Mean flow angles were calculated as arctan(W/U), and here the effect of the flow distortion correction was on average 1.3° and 0.3° for the Solent R2 (both schemes) and USA-1 sonic respectively.

After the corrections, the mean daily course of W by the two sonic anemometers agreed better.

4.3 Flow angle dependence on wind direction for near-neutral subset

In order to understand the possible terrain effect on the sonic measurements, the flow angles were calculated as a function of wind direction for the Solent R2 and the USA-1 sonic anemometers for both a winter and a summer period (Fig. 6). Only near-neutral data was chosen for this analysis and flow distortion corrections were applied. For the Solent R2 sonic, the numerically improved version of the correction was used ("corr 2"). The thick red line shows the centered running mean of 50 samples. The vertical dashed line indicates the direction of the mast from the boom at 130°.

During the summer, the flow patterns measured by the two sonic anemomters were rather similar (Fig. 6, top), with a pronounced minimum of −1° to −2° around 270°, a less pronounced minimum around 110° and weak maxima around 60° and 160°.

The flow angles from the Gill sonic are slightly lower than the Metek sonic in the interval [330°, 100°]. This difference could be due to a small relative misalignment between the sonic anemometers or an effect caused by the different measurement heights.

The good agreement between the directional flow pattern from the two sonic anemometers disappear during the winter period (Fig. 6, bottom). Whereas the main features from the summer were preserved for the Metek sonic, the Gill sonic flow pattern was changed with more negative flow angles in the northeast and less negative flow angles in the southwest. Flow angles from both sonic anemometers showed a more varying pattern, with many local maxima and minima. These features were still common for the two instruments. For example, three local maxima around 200°, 250° and 315° appear for both sonics. These local maxima were not as pronounced for the summer data.

Generally, the flow angles from the Metek sonic were more negative during winter than summer.

The squared correlation coefficient (R^2) for near-neutral data from the two sonic anemometers was 0.25 for the summer period and 0.18 for the winter period.

4.4 Flow angle dependence on atmospheric stability and wind direction

The analysis in the previous subsection was extended for the summer case to include an unstable and a stable dataset. The result is shown in Fig. 7, where the full line is the neutral data, the dashed line represent stable conditions and the dotted line shows the unstable data. Only the 50 samples running mean curve is shown, in order to be able to distinguish the main feature of the flow pattern. The stable and unstable subset were much smaller than the neutral data, with 738 stable samples and 238 unstable samples compared to the 2150 neutral samples. The scatter for the half-hourly samples was evaluated for the [250°, 280°] interval to σ_{α_n}=0.7°, σ_{α_s}=0.6° and $\sigma_{\alpha_{us}}$=2.0°, where subscripts *n*, *s* and *us* denote the neutral, stable and unstable subset respectively. The high value for the unstable subset was partly caused by a too small sample size (25 samples). By widening the interval to [230°, 300°], $\sigma_{\alpha_{us}}$ was reduced to 1.6°.

Relative to the neutral data, the flow angles from the Solent R2 during stable conditions were predominantly more negative or more positive, depending on whether the flow distortion correction by van der Molen et al. (2004) or Nakai et al. (2006) was applied. For both flow distortion corrections as well as the raw data, the flow angles during unstable conditions were more positive than during neutral conditions. For the USA-1 sonic anemometer, the flow distortion corrected unstable dataset was following the neutral subset more closely than for the Solent-R2.

Common features in all three graphs in Fig. (7) were that the stable subset gave lower flow angles in sector [0°, 90°] and that the stable subset followed the neutral in the southern and wester sector.

Uncorrected data from the Solent R2 were qualitatively similar to the "Corr 2" scheme, and the difference between the uncorrected and the corrected scheme for the USA-1 was minor.

4.5 Analysis of lidar data

In contrast to the data from Høvsøre, the vertical velocities from conically scanning lidar data at Sorø showed no sinusoidal behavior at the furthest measurement height of 177 m (Fig. 8, lower right), which implies that the instrument was well aligned to the surface. For the western and southern directions relative to the mast, the lidar flow angles were between −1° and −2°, which is very similar to the winter result of the USA-1 sonic by Metek.

The variation in the horizontal flow field deduced from the linearly scanning lidar is shown in Fig. 9. Each point represents a mean value over 97 half hours of scanning. Near-neutral data from the western sector of the forest ([250°, 280°]) were selected to match the lidar scanning direction of 270° and provide a uniform forest fetch. The vertical bars show the standard deviation of the wind. The flow showed an apparent random variation of about 1.3% (left), but no systematic horizontal gradient. The continuity equation for two-dimensional flows $W = -\int_0^{z_m} \frac{dU}{dx} dz$ was used to derive $W = -\Delta U \Delta x \cdot z_m / 2$ where z_m=38 m and dU/dx is assumed to be a linear function of height with boundary conditions $dU/dx = 0\,\mathrm{s}^{-1}$ at z=0 m and $dU/dx = \Delta U/\Delta x\,\mathrm{s}^{-1}$ at z_m=38 m, where Δx denotes the distance between two focus points. To the right in Fig. 9, two derived vertical velocities using the focus points 36 m and 61 m, and 20 m and 55 m are plotted against each other. The mean value of the two derived vertical velocities were $W_{55\,\mathrm{m},20\,\mathrm{m}} = 0.05\,\mathrm{ms}^{-1}$ and $W_{61\,\mathrm{m},30\,\mathrm{m}} = 0.008\,\mathrm{ms}^{-1}$. The corresponding standard deviations were $\sigma_{W_{55\,\mathrm{m},20\,\mathrm{m}}} = 0.7\,\mathrm{ms}^{-1}$ and $\sigma_{W_{61\,\mathrm{m},30\,\mathrm{m}}} = 0.6\,\mathrm{ms}^{-1}$. The correlation between the two derived vertical velocities was low with R^2=0.036.

5 Discussion

5.1 The effect of flow distortion corrections

The flow distortion correction from the sonic structure led to a large negative shift of vertical velocities and flow angles for the Solent R2 sonic, whereas it led to a positive shift of vertical velocities and flow angles for the USA-1 sonic (Fig. 5). The reason for the strong negative shift of the Solent R2 signals is that negative vertical velocities generally were corrected more than the positive vertical velocities.

Contrary to the Solent R2, the flow distortion correction supplied by Metek Gmbh for the USA-1, does not cover the whole ($-90^\circ, 90^\circ$) interval, and this correction is therefore not complete. A study by Högström and Smedman (1989) pointed to a difference of the flow distortion corrections achieved in wind tunnels with laminar flow compared to the necessary correction for the turbulent atmospheric flow using Gill R2 and R3 instruments. They also found that Solent R2/R3 correction schemes for different individual anemometers were non-identical. It therefore seems likely that neither of the applied corrections schemes perfectly reflects the real distortion by the anemometer structure. However, a positive off-set in flow angles seems to be a general feature of the Solent sonic anemometer (Heinesch et al., 2007; Wilczak et al., 2001) and as it improved the agreement with the USA-1, it seems likely that the correction improved the precision of the anemometer.

It is difficult to assess the final precision of the sonic anemometers. Taking the effect of the flow distortion schemes as an indirect rough estimate of the precision, we estimate that the precision of the vertical velocity was in the order of 0.01 ms^{-1} to 0.1 ms^{-1} depending on what type instrument is used. Similarly for flow angles, the precision should not be considered better than $0.5^\circ - 1^\circ$.

For the Solent R2, the data taken during stable conditions showed flow angles either more negative of more positive than the neutral flow angles depending on what flow distortion scheme was applied (Fig. 7). The small difference between the corr1 and corr2 calibration schemes still had significant effects. Since the probability function of the angle of attack on the sonic depends on atmospheric stability as shown in Fig. 4, the flow distortion correction affects different atmospheric stabilities differently and if a standard advection rotation relative to the neutral flow angles had been applied, as done in most of the cited advection studies, we could either have achieved rather small positive or negative vertical velocities depending on which of the two corrections was applied. Instrumental uncertainties due to flow distortion can not – unless the calibration scheme is absolutely perfect – be easily removed by assuming that the neutral data defines the zero-flow angle surface.

5.2 Limitation of sonic anemometer accuracy due to statistical uncertainty

One of the main conclusion of Feigenwinter et al. (2008), was that sonic based vertical advection estimates should not be applied on a half-hourly basis. In the light of the data presented in Table 2, this conclusion is very natural as the statistical deviation of the vertical velocity estimate is many times greater than the expected signal. With the current setup, and in order to reach the accuracy limit of 1 mm s^{-1} stated by Leuning et al. (2008), stationary time series of more than 100 days duration would be necessary. A more robust alternative to using measured W for each half hour average, could be to calculate a mean flow angle for the wind direction of interest, which was based on an ensemble of the single-run flow angles. This would reduce the scatter significantly.

5.3 Linearly scanning lidar

Although the assumption of linearly declining divergence with height may not hold for the calculation of W in Fig. 9, the results still point towards at least two difficulties in determining W from wind speed differences: (1) Mean values over the 97 samples could give rise to both positive and negative mean horizontal gradients depending on

BGD
6, 8167–8213, 2009

what focus points were chosen indicating large spatial variability and (2) the horizontal variation of the flow was many times greater than the gradient associated with flow angle of a couple of degrees. This led to derived values of mean vertical velocities near 0.5 ms^{-1}, which is nearly an order of magnitude greater than the measured W from the sonic anemometers. An explanation for the large magnitude of the derived vertical velocities is the neglect of the transversal wind component in the derivation.

An instrumental problem with the linearly scanning lidar, is the difficulty of aligning the sensor in parallel with the underlying surface. In order to use a continuity approach for above canopy flows, we estimate that much greater distances are needed in order to find a systematic deceleration or acceleration of the flow, such that small alignment errors can be neglected. Vickers and Mahrt (2006) successfully utilizes a set of towers 200 m apart to derive vertical velocities from the continuity approach including both the mean wind and the transversal component of the flow. In the studies by Leuning et al. (2008); Heinesch et al. (2007) towers at a distance of 50 and 90 m respectively are used to measure below canopy wind gradients which in turn are used to derive W.

5.4 Comparison of flow angles

In Fig. 10, the 50 sample running mean averages were plotted for the summer experiment (top) and the winter experiments (middle and bottom). For the winter sonic-sonic comparison, the disagreement between the two anemometers shown in the previous section could be compensated by a small tilt of the Solent. By applying a 1° tilt to the measured data, the comparison in the western sector became equally good as for the summer and the disagreement between the instruments in the northeastern directions were also similar to the summer. We speculate that the less robust Solent anemometer may have been flexed due to higher wind loads during winter, which could explain the tilt.

The agreement between the two lowest focus distances by the lidar at 50 and 60 m agree rather well with the flow pattern by the USA-1 (bottom), except for the direction of 180°. The systematic error in the vertical lidar-derived velocity due to inhomogeneity of the flow was estimated to be less than 20% and will not change the results significantly. Due to the limited extension of the lidar experiment, flow angles from all wind direction could unfortunately not be sampled, and the good agreement between the lidar and the sonic in Fig. 10 may be a coincidence. However, the result is encouraging and further campaigns should prove the usefulness of the ground based remote sensing lidars also for mean vertical velocities and flow angles.

5.5 Interpretation of flow angles in relation to the terrain

It is possible to relate the flow angles in Fig. 10 with features of the terrain at the Sorø site in combination with the presented conceptual model for flow angles near a forest edge in Fig. 1. For the summer data, the local maxima around 60° and 160° could be related to the acceleration and deceleration phases for features 1 and 3 defined in Fig. 3. The local minima around 270° and 110° could similarly be related to either an interaction phase for feature 6 or an effect of a trailing edge for feature 7. This would mean that the deceleration phase (Fig. 1), extends to at least $8h_c$ during summer time. For the winter case, the local maxima in Fig. 10 (middle) can be related to acceleration or deceleration phases for features 4, 5 and 7. Since these features are located further from the mast than features 1 and 3, this would point towards a slower adaptation of the step change in vegetation during winter time than during summer time. This could in turn be explained by the edge being more porous during winter, thereby letting more flow go through it and slowing up the adaptation.

As the instrumental uncertainties were of such large magnitude relative to the measured variation in flow angles, and we further have assumed that the surface parallel to the canopy top followed the ground surface perfectly, this detailed interpretation of the absolute values of the flow angles in relation to the terrain is uncertain. Some features in Fig. 10 may therefore also be influenced by a sloping canopy top or smaller scale variations in the ground surface inclination.

The flow angles were more positive during un-stably stratified flows than for neutrally stratified flow (both sonic anemometers) and followed the neutral mean curve to some extent, whereas the results for stable subset was closer to the neutral. Using the internal boundary layer concept, this could be explained by the expected faster growth of IBL for unstably stratified flows (Rao, 1975; Kaimal and Finnigan, 1994).

Instead of relating the non-zero flow angles to larger-scale temperature driven circulation as in Lee (1998), these results point to an alternative interpretation, namely that the vertical velocities in complex terrain/terrain with inhomogeneous surface cover during stably and unstably stratified flows follow the terrain – or the surface defined by the canopy crowns – differently than under neutral conditions.

5.6 Implications for vertical advection estimates at fetch-limited sites and sites with clearings

If systematic vertical advection caused by flow adaption to the terrain should be included in the carbon budget of the surface, advective flows would be of greater importance than previously estimated. To illustrate this, we have constructed an example based on the presented results.

For the summer data, data from both sonic anemometers showed a well-defined minimum around 270°, which corresponds to the wind direction of a homogeneous fetch for approximately 500m. Turbulent carbon dioxide flux data at near-neutral conditions from the direction interval [250°, 280°] and carbon dioxide profile data from the summer of 2007 were used to assess the potential effect of systematic advection. The advection term was evaluated following Lee (1998) as

$$\int_0^{z_m} W(z)\frac{\partial C}{\partial z}dz = W_{z_m}\left(C_{z_m} - z_m^{-1}\int_0^{z_m} C(z)dz\right). \tag{12}$$

For $C(z)$ a piecewise constant measured values of the CO_2 gradient was used in the integration.

In Fig. 11, the mean daily course of the estimated fluxes are presented. Here we have used a hypothetical case of a mean wind speed of $4\,\mathrm{ms}^{-1}$ and mean flow angles of $-0.5°$ to $-1°$. Compared to the turbulent flux, the advection term during night time would enhance the total flux by as much as 25–50%, whereas the day time enhancement would not be greater than 25%. To calculate this example, only neutral data was considered.

A common argument for not including the large vertical advection term, is that a horizontal advection term would balance out the vertical advection leading to a near-zero advection contribution (Feigenwinter et al., 2004; Aubinet et al., 2005). A large horizontal advection term of opposite sign as the vertical is of course also a possibility that can not be ruled out for this study.

However, disregarding the horizontal advection term, we still find it questionable to include the vertical advection term, which represents such a large correction to the eddy-covariance flux. Since W can change sign as an effect of local surface heterogeneities, the vertical advection term estimated at the mast will not be representative for the whole forest.

Given this argument, we would like to extend the conclusion by Feigenwinter et al. (2008), that the vertical advection term should not be included at a half-hourly time scale, to question whether the term should ever be included if the surface cover is heterogeneous.

6 Conclusions

An analysis of mean vertical velocities and flow tilt angles from 3-D sonic anemometers and a ground based remote sensing wind lidar was presented. For the sonic anemometers (Solent Gill R2 at and Metek USA-1), flow distortion correction schemes were applied to account for how the sonic itself affects the measured flow. It was found that the flow distortion correction affects the mean flow angles significantly. For the Solent R2, the mean value of the vertical velocity over all stabilities and wind directions changed from being positive to negative. As the corrections were dependent on sonic attack angle distribution, which varies with atmospheric stability, the flow distortion correction affected vertical velocities during different atmospheric stability differently. Relative to

BGD
6, 8167–8213, 2009

the flow angles during neutral atmospheric stratification, the flow angles during non-neutral conditions changed from being predominantly positive to negative depending on which flow distortion correction was applied.

The statistical uncertainty of the 30 min mean vertical velocities was estimated using sonic anemometer data and was found to be of large magnitude relative to expected mean values of the vertical velocity. The estimated statistical uncertainty fit well with the actual scatter of half-hourly averages of measured flow angles. A horisontal linearly scanning lidar mounted on the mast showed the spatial variation of the flow field. The apparent random variation of the flow of 1.3% resulted in a derived vertical velocity almost an order of magnitude greater than the vertical velocities measured by the sonic anemometers. Based on these data, the calculation of vertical velocities from a continuity approach was discussed.

Flow angles from eight heights between 50 m and 177 m were also calculated from a conically scanning lidar, which was based on top of a scaffolding tower near the mast. The vertical velocity was deduced by assuming horisontal homogeneity. The violation of the horisontal homogeneity assumption was estimated to cause a relatively small error to the derived vertical velocity. As this technique is novel, measurements from the forest site were compared with measurements at a flat low-vegetation site. It was found that flow angles from the forest site showed more variation than at the flat low-vegetation site. The standard deviation of the derived vertical velocity was of similar size as the vertical velocities from the sonic anemometers.

Since the forest site is fetch-limited and contains clearings, non-zero flow angles were expected even during neutral atmospheric stratification. The dependence of the measured flow angle on wind direction was therefore analyzed. Instead of using a tilt-rotation algorithm where flow angles were assumed to be zero for neutral conditions, as has been done in most vertical advection studies, the coordinate system defined by the sonic anemometers and lidar were used.

Both positive and negative flow angles were found, which could be related to either a clearing within the forest, the limited fetch of the forest or a trailing edge downwind of the mast. A simple conceptual model explaining the non-zero flow angles was presented. The directional dependence and the magnitude of the flow angles from the conically scanning lidar and the sonic anemomters match reasonably well.

Generally, all presented methods for assessing vertical mean velocities and flow angles must be considered uncertain and at the limit of what can be measured experimentally.

The vertical advection term based on a single point measurement was estimated for the western sector of the forest. However, it was not recommended to include this term in connection with the measured flux, as the vertical velocity measured at the mast is not representative for the whole forest.

Acknowledgements. The authors would like to acknowledge Søren Larsen, Niels Otto Jensen (at the Wind Energy Division at Risø-DTU) and Gunnar Schade (at the Department for Atmospheric Sciences, Texas A&M University) for valuable comments on the manuscript. This work is financed through the UPWIND project (WP6) funded by the European Commission, the NECC project funded by the Nordic Natural Science Research Councils (NOS-N), and the Forest and Wind Profile project funded by the Danish Strategic Research Council.

References

Aubinet, M., Berbigier, P., Bernhofer, C., Cescatti, A., Feigenwinter, C., Granier, A., Grunewald, T., Havrankova, K., Heinesch, B., Longdoz, B., Marcolla, B., Montagnani, L., and Sedlak, P.: Comparing CO_2 storage and advection conditions at night at different CarboEuroflux sites, Boundary Layer Met., 116, 63–94, 2005. 8169, 8194

Baldocchi, D., Finnigan, J., Wilson, K., Paw, U. K., and Falge, E.: On measuring net ecosystem exchange over tall vegetation on complex terrain, Bound.-Lay. Meteorol., 96, 257–291, 2000. 8169, 8171

Baldocchi, D., Falge, E., Gu, L., Ohlson, R., Hollinger, D., Running, S., Anthoni, P., Bernhofer, C., Davis, K., Evans, R., Fuentes, J., Goldstein, A., Katul, G., Law, B., Lee, X., Malhi, Y., Meyers, T., Munger, W., Oechel, W., Paw U, K., Pilegaard, K., Schmid, H., Valentini, R., Verma, S., Vesala, T., Wilson, K., and Wofsy, S.: FLUXNET: A new tool to study the temporal and spatial variability of ecosystem-scale carbon dioxide, water vapor and energy flux densities, B. Am. Meteorol. Soc., 82, 2415–2434, 2001. 8169

Belcher, S. and Hunt, J.: Turbulent flows over hills and waves, Ann. Rev. Fluid Mech., 30, 507–538, 1998. 8173

Belcher, S., Finnigan, J., and Harman, I.: Flows through forest canopies in complex terrain, Ecol. Appl., 18, 1436–1453, 2008. 8173

Bingöl, F., Mann, J., and Foussekis, D.: Modeling conically scanning lidar error in complex terrain with WAsP Engineering, Meteorol. Z., 18, 189–195, 2009. 8178

Cassiani, M., Katul, G., and Albertson, J.: The effects of canopy leaf area index on airflow across forest edges: large-eddy simulation and analytical results, Bound.-Lay. Meteorol., 126, 433–460, 2008. 8175

Courtney, M., Wagner, R., and Lindelöw, P.: Testing and comparison of lidars for profile and turbulence measurements in wind energy, IOP Conference Series: Earth and Environmental Science, 1, 012 021 (14 pp.), http://stacks.iop.org/1755-1315/1/012021, 2008. 8176

Davis, J. C., Collier, C. G., Davies, F., Pearson, G. N., Burton, R., and Russell, A.: Doppler lidar observations of sensible heat flux and intercomparisons with a ground-based energy balance station and WRF model output, Meteorol. Z., 18, 155–162, 2009. 8170

Dellwik, E. and Jensen, N.: Internal equilibrium layer growth over forest, Theor. Appl. Climatol., 66, 173–184, 2000. 8172

Dellwik, E. and Jensen, N.: Flux-profile relationships for a fetch limited beech forest, Bound.-Lay. Meteorol., 115, 179–204, 2005. 8172, 8180, 8181

Feigenwinter, C., Bernhofer, C., and Vogt, R.: The influence of advection on the short term CO2 budget in and above a forest canopy, Bound. Lay. Meteorol., 113, 201–224, 2004. 8169, 8171, 8194

Feigenwinter, C., Bernhofer, C., Eichelmann, U., Heinesch, B., Hertel, M., Janous, D., Kolle, O., Lagergren, F., Lindroth, A., Minerbi, S., Moderow, U., Mlder, M., Montagnani, L., Queck, R., Rebmann, C., Vestin, P., Yernaux, M., Zeri, M., Ziegler, W., and Aubinet, M.: The influence of advection on the short term CO2 budget in and above a forest canopy, Agric. For. Meteorol., 148, 12–24, 2008. 8169, 8171, 8194

Finnigan, J.: A comment on the paper by Lee (1998): On micrometeorological observations of surface-air exchange over tall vegetation, Agric. For. Meteorol., 97, 55–64, 1999. 8169, 8171

Gash, J. and Dolman, A.: Sonic anemometer (co)sine response and flux measurement I. The potential for (co)sine error to affect sonic anemometer-based flux measurements, Agric. For.

BGD

6, 8167–8213, 2009

Mean vertical velocities and flow tilt angles at a fetch limited forest site

E. Dellwik et al.

Meteorol., 119, 195–207, 2003. 8182
Heinesch, B., Yernaux, M., and Aubinet, M.: Some methodological questions concerning advection measurements: a case study, Bound. Lay. Meteorol., 122, 457–478, 2007. 8169, 8172, 8182, 8189, 8191
Högström, U. and Smedman, A.-S.: Accurace of sonic anemometers: laminar wind-tunnel calibrations compared to atmospheric in-situ calibrations against a reference instrument, Bound.-Lay. Meteorol., 111, 33–54, 1989. 8189
Irvine, M., Gardiner, B., and Hill, M.: The evolution of turbulence across a forest edge, Bound.-Lay. Meteorol., 84, 467–496, 1997. 8174
Kaimal, J. and Finnigan, J.: Atmospheric boundary layer flow, their structure and measurement, Oxford University Press, 289 pp., 1994. 8193
Kutsch, W., Kolle, O., Rebmann, C., Knohl, A., Ziegler, W., and Schulze, E.-D.: Advection and resulting CO_2 exchange uncertainty in a tall forest in central Germany, Ecol. Appl., 18, 1391–1405, 2008. 8169, 8171
Lee, X.: On micormeteorological observations of surface-air exchange over tall vegetation, Agric. For. Meteorol., 91, 39–49, 1998. 8169, 8171, 8173, 8193
Lenschow, D. H., Mann, J., and Kristensen, L.: How Long Is Long Enough When Measuring Fluxes and Other Turbulence Statistics?, J. Atmos. Ocean. Technol., 11, 661–673, 1994. 8170, 8175, 8178
Leuning, R., Zegelin, S., Jones, K., Keith, H., and Hughes, D.: Measurement of horizontal and vertical advection of CO2 within a forest canopy, Agr. For. Meteorol., 148, 1777–1797, 2008. 8169, 8172, 8190, 8191
Lothon, M., Lenschow, D. H., and Mayor, S. D.: Coherence and scale of vertical velocity in the convective boundary layer from a Doppler lidar, Bound.-Lay. Meteorol., 121, 521–536, 2006. 8170
Mammarella, I., Kolari, P., Rinne, J., Keronen, P., and Vesala, T.: Determining the contribution of vertical advection to the net ecosystem exchange at Hyytiala forest, Finland, Tellus, 59B, 900–909, 2007. 8169
Mammarella, I., Dellwik, E., and Jensen, N.: Turbulence spectra, shear-stress and tubulent kinetic energy budgets above two beech forest sites in Denmark, Tellus B, 60, 179–187, 2008. 8171, 8172
Mann, J., Cariou, J.-P., Courtney, M. S., Parmentier, R., Mikkelsen, T., Wagner, R., Lindelöw, P., Sjöholm, M., and Enevoldsen, K.: Comparison of 3D turbulence measurements using three

staring wind lidars and a sonic anemometer, Meteorol. Z., 18, 135–140, 2009. 8170
McMillen, R.: An eddy correlation technique with extended applicability to non-simple terrain, Bound.-Lay. Meteorol., 43, 231–245, 1988. 8184
Morse, A., Gardiner, B., and Marshall, B.: Mechanisms controlling turbulence development across a forest edge, Bound.-Lay. Meteorol., 103, 227–251, 2002. 8174
Nakai, T., van der Molen, M., Gash, J., and Kodama, Y.: Correction of sonic anemometer angle of attack errors, Agric. For. Meteorol., 136, 19–30, 2006. 8182, 8185, 8187
Paw, U. K., Baldocchi, D., Meyers, T., and Wilson, K.: Correction of eddy-covariance measurements incorporating both advective effects and density fluxes, Bound.-Lay. Meteorol., 97, 487–511, 2000. 8169, 8171
Pilegaard, K., Mikkelsen, T., Beier, C., Jensen, N., Ambus, P., and Ro-Poulsen, H.: Field measurements of atmosphere-biosphere interactions in a Danish beech forest, Boreal Environ. Res., 8, 315–333, 2003. 8180, 8181
Rao, K.: Effetct of thermal stratification on the growth of the internal boundary layer, Bound.-Lay. Meteorol., 8, 227–234, 1975. 8193
Smith, D. A., Harris, M., Coffey, A. S., Mikkelsen, T., Jørgensen, H. E., Mann, J., and Danielian, R.: Wind lidar evaluation at the Danish wind test site Høvsøre, Wind Energy, 9, 87–93, 2006. 8176, 8179
Smith, F., Carson, D., and Oliver, H.: Mean wind direction shear through a forest canopy, Boundary-Layer Meteorol., 3, 178–190, 1972. 8173
Sogachev, A., Rannik, Ü., and Vesala, T.: Flux footprint over complx terrain covered by heterogeneous forest., Agric. For. Meteorol., 127, 143–158, 2004. 8173
Sogachev, A., Leclerc, M., Zhang, G., Rannik, U., and Vesala, T.: CO2 fluxes near a forest edge: a numerical study, Ecol. Appl., 18, 1454–1469, 2008. 8174
Thom, A.: Momentum absorption by vegetation, Q. J. Roy. Meteorol. Soc., 97, 414–428, 1971. 8170
van der Molen, M., Gash, J., and Elbers, J.: Sonic anemometer (co)sine response and flux measurement II. The effect of introducing an angle of attack dependent calibration, Agric For. Meteorol., 112, 95–109, 2004. 8182, 8185, 8187
Vickers, D. and Mahrt, L.: Contrasting mean vertical motion from tilt correction methods and mass coninuity, Agr. For. Meteorol., 138, 93–103, 2006. 8169, 8172, 8191
Wilczak, J., Oncley, S., and Stage, S.: Sonic anemometer tilt corrections algorithms, Bound.-Lay. Meteorol., 99, 127–150, 2001. 8189

Yang, B., Raupach, M., Shaw, R., U, K., and Morse, A.: Large-eddy simulation of turbulent flow across a forest edge. Part1: Flow statistics, Bound.-Lay. Meteorol., 120, 377–412, 2006. 8175

Yi, C., Anderson, D., Turnipseed, A., Burns, S., Sparks, J., Stannard, D., and Monsoon, R.: The contribution of advective fluxes to net ecosystem exchange in a high-elevation, subalpine forest, Ecol. Appl., 18, 1379–1390, 2008. 8169, 8171

Table 1. Overview of experiments and sites used for instrument intercomparison. The measurement height denotes the height above the ground for the sonic anemometers and the conically scanning lidar, and the focus distance from the mast for the linearly scanning lidar.

Dataset	Duration of experiment	Measurement height/focus distance (m)
Sorø "summer"	1 Jun 2005–31 Aug 2005	43 m Gill R2, 31.5 m Metek USA-1
Sorø "winter"	18 Jan 2005–1 May 2005	43 m Gill R2, 31.5 m Metek USA-1
Conically scanning lidar	15 Nov 2006–6 Jan 2006	50, 59, 67, 78, 94, 115, 89, 142, 177
Linearly scanning lidar	25 Jan 2007–4 Feb 2007	20, 25, 30, 36, 40, 45, 50, 55, 61

Table 2. Statistical uncertainties evaluated for $T=1800$s and measured mean values of $|W|$ and σ_w/U from the flow distortion corrected Solent sonic anemometer for varying atmospheric stratification.

Subset	$\frac{\sigma_w}{U}$ (–)	σ_{W_T} ($\mathrm{ms^{-1}}$)	σ_{α_T} (°)	$\lvert W_{\mathrm{Solent}}\rvert$ ($\mathrm{ms^{-1}}$)
Near-neutral	0.19	0.07	0.8	0.07
Stable	0.08	0.02	0.4	0.04
Unstable	0.24	0.05	1.4	0.06

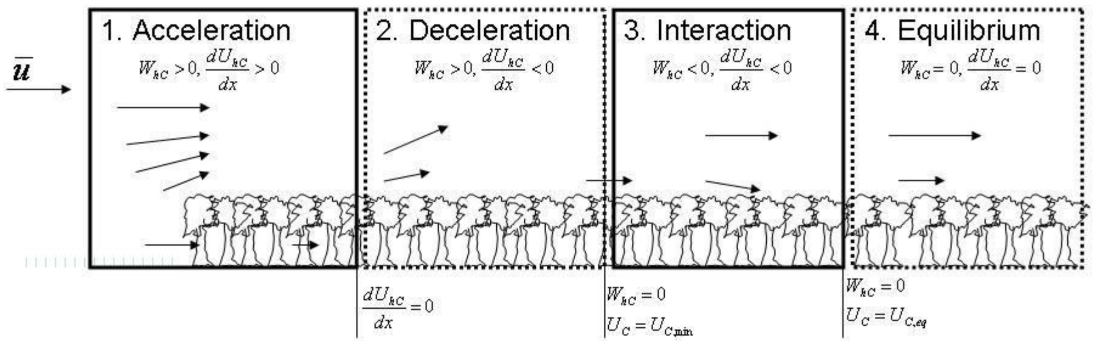

Fig. 1. Sketch of flow downstream of a forest edge.

BGD

6, 8167–8213, 2009

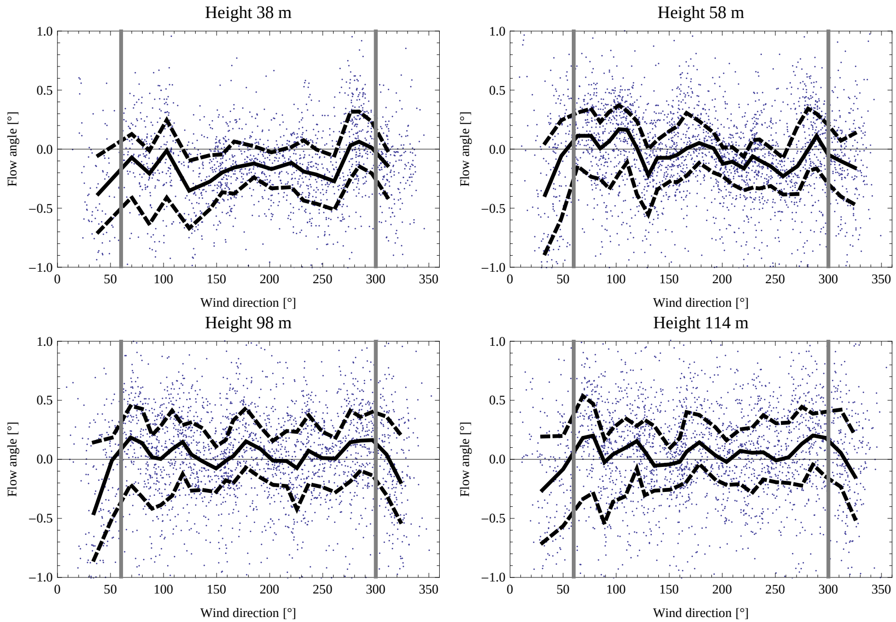

Fig. 2. Half hour averages of the flow angle measured by lidar at a very flat site. The solid lines are binned median values, and the dashed are 25% and 75% quantiles, respectively. Between the vertical gray lines the flow is undisturbed by the wind turbine array.

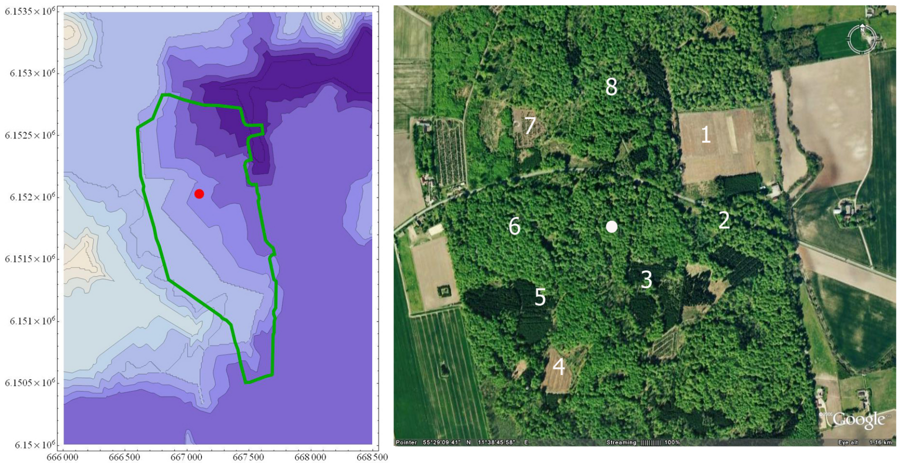

Fig. 3. Map and photography of the Sorø site. The height contours (right) signifies 2 m height differences.

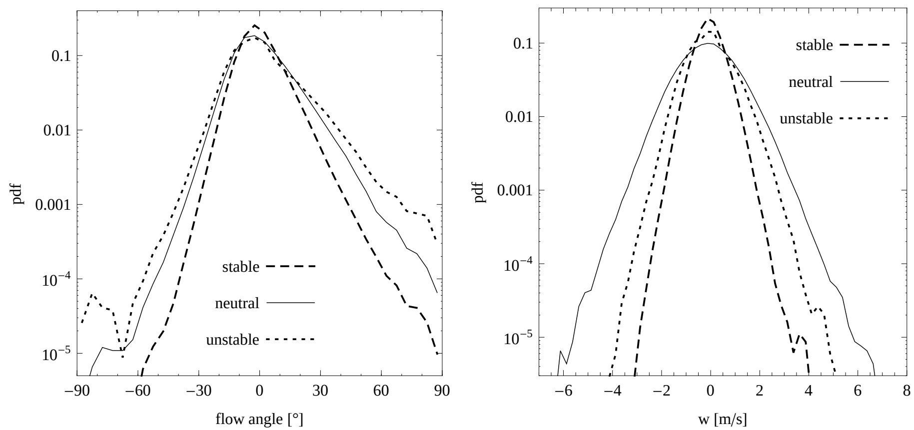

Fig. 4. Probability density of attack angle on sonic anemometer and vertical velocities for three atmospheric stability subsets based on 10 Hz data.

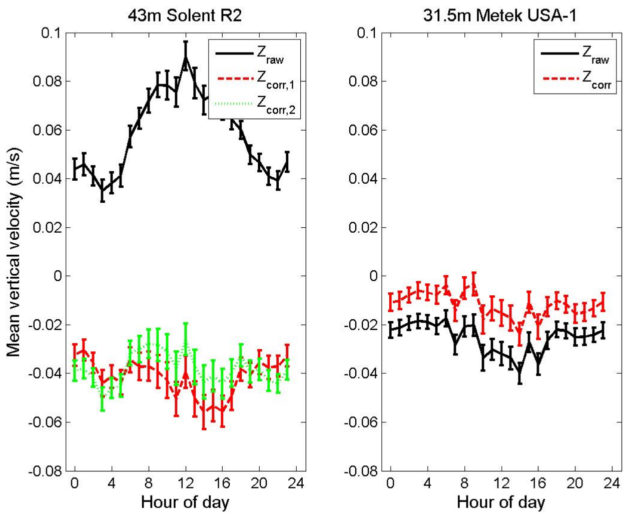

Fig. 5. Effect of flow distortion corrections on mean daily courses of vertical velocities for all wind directions and stabilities.

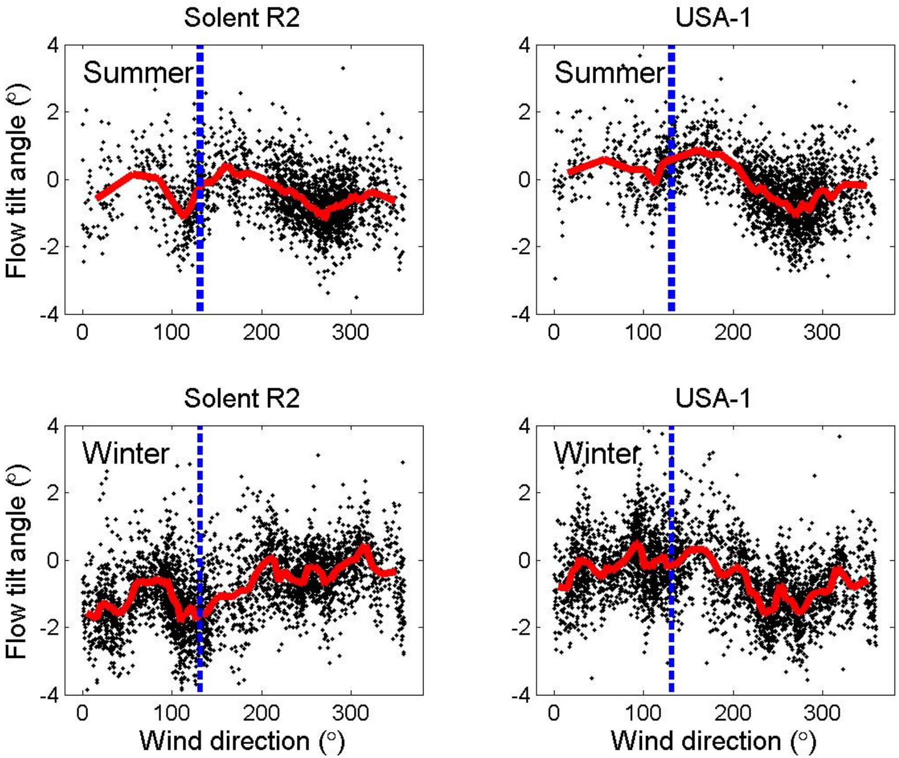

Fig. 6. Neutral data tilt angle during full leaf area index conditions (top) and low leaf area index conditions (bottom).

BGD
6, 8167–8213, 2009

Title Page
Abstract
Introduction
Conclusions
References
Tables
Figures
◂
▸
Back
Close
Full Screen / Esc
Printer-friendly Version
Interactive Discussion

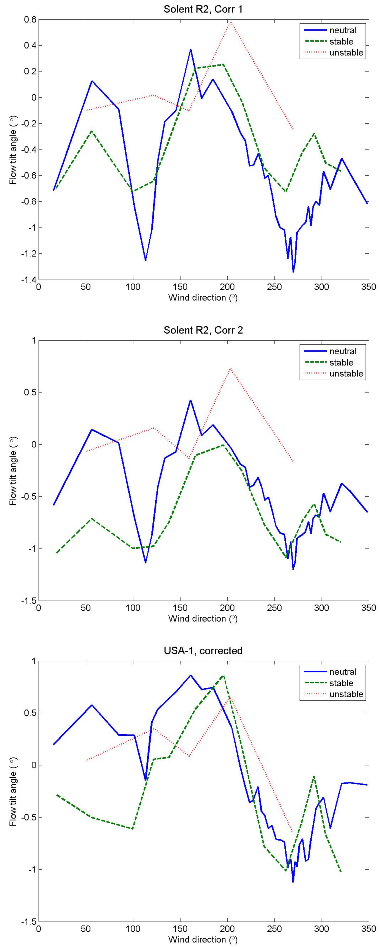

Fig. 7. Directional response of neutral, stable and unstable dataset for the summer of 2005.

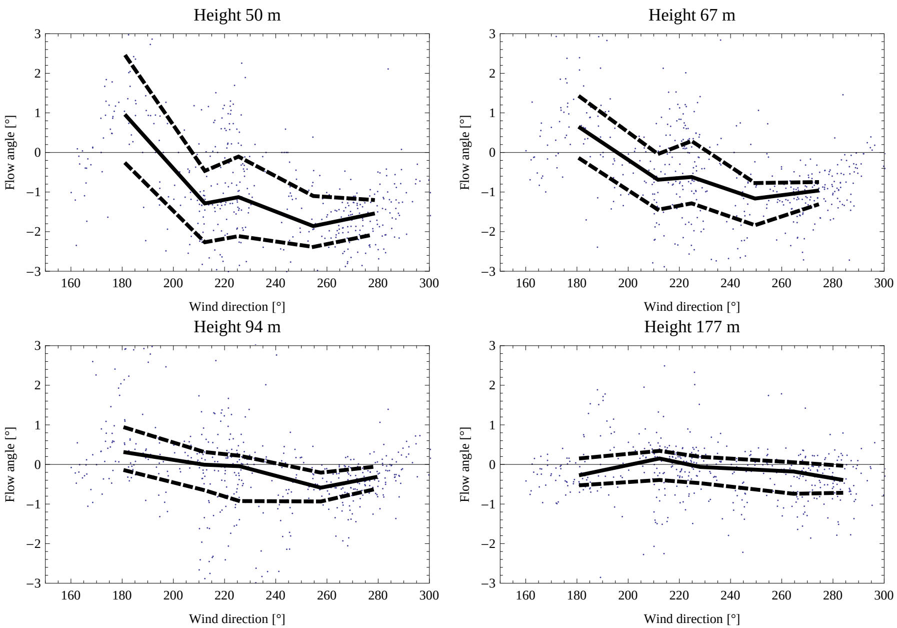

Fig. 8. Half hour averages of the flow angle measured by lidar at Sorø during the late autumn and winter of 2006–2007. The solid lines are binned median values, and the dashed are 25% and 75% quantiles, respectively.

BGD

6, 8167–8213, 2009

Mean vertical velocities and flow tilt angles at a fetch limited forest site

E. Dellwik et al.

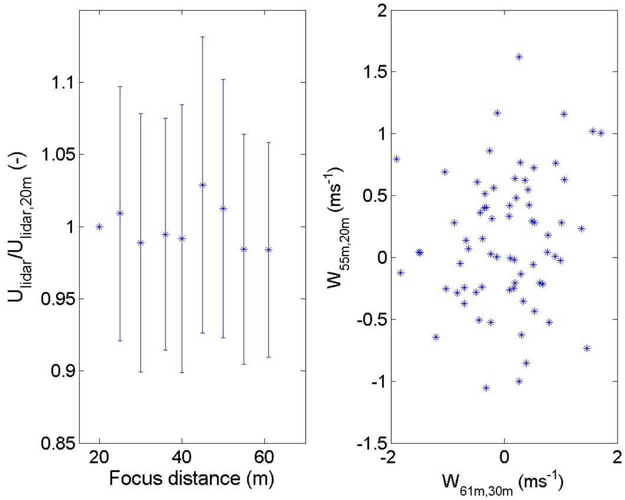

Fig. 9. Horizontal variation in the mean wind speed as measured by the mast-mounted lidar (left) and derived mean vertical velocities from a continuity approach (right).

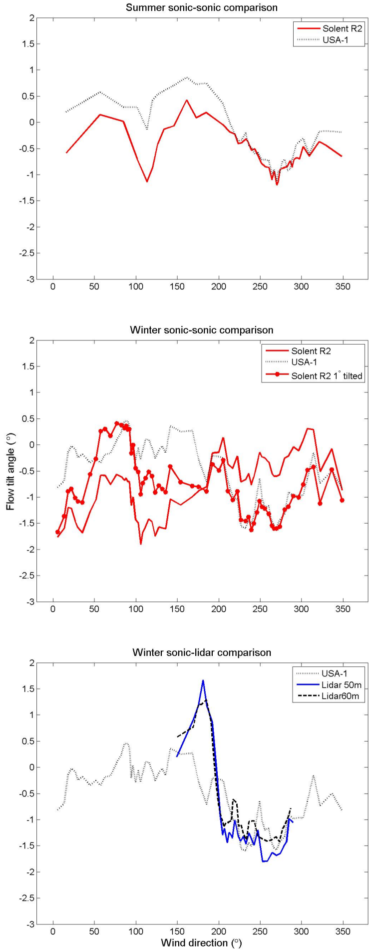

Fig. 10. Comparison of direction response for the two sonic anemometers (top and middle) and the conically scanning lidar (bottom).

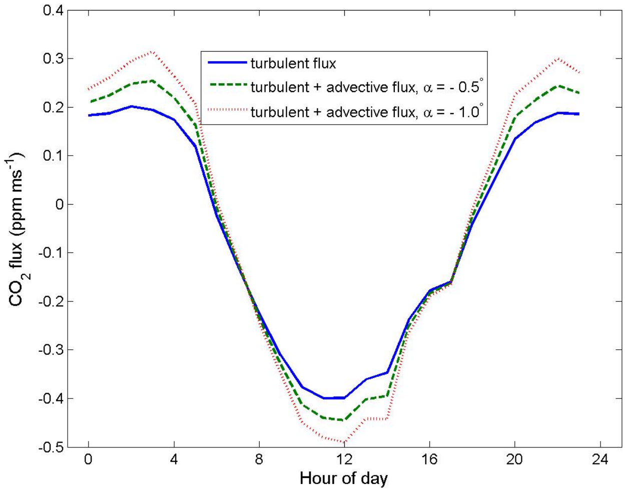

Fig. 11. Sensitivity analysis of the contribution of the vertical advection term to the measured turbulent eddy-flux during near-neutral conditions.